JOURNAL OF SOLID STATE CHEMISTRY 91, 238–249 (1991)

Local Environment of Iron in Heavy Ion-Irradiated Amorphous Magnetic Oxides by Mössbauer and X-Ray Absorption Spectroscopy

F. STUDER,* CH. HOUPERT,* M. TOULEMONDE,† AND E. DARTYGE‡

*CRISMAT, ISMRa, 14032 Caen Cedex; †CIRIL, CEA-CNRS, 14040 Caen Cedex; and ‡LURE, CNRS-CEA-MEN, 91405 Orsay Cedex, France

Received July 5, 1990; in revised form November 1, 1990

Mössbauer and X-ray absorption spectroscopies of some crystallized iron oxides, Fe_2O_3, $FePO_4$, Fe_3PO_7, and $SrMn_{1.85}Fe_{0.15}O_{2.5}$, the garnet $Y_3Fe_5O_{12}$, and the barium hexaferrite $BaFe_{12}O_{19}$ have been undertaken in order to look at the local order around iron in $Y_3Fe_5O_{12}$ and $BaFe_{12}O_{19}$ materials amorphized by irradiation with high energy (27 MeV/n) xenon ions accelerated by GANIL. Simulations of the Mössbauer spectra suggested the presence of fivefold coordinated iron in the amorphous irradiated compounds with a distribution of magnetic interactions due to the variations of the number of iron second neighbors. The XANES spectra at the Fe–K edge confirmed the fivefold coordination of iron in the amorphous ferrites, show that the local structure around iron appears to be similar although the original structures were different, and appear close to the one observed in the Fe_3PO_7 compound in which iron stands in a trigonal bipyramidal environment. EXAFS simulations gave Fe–O distances of 1.95 Å intermediate between Fe–O distances in octahedral (1.97 Å) and tetrahedral (1.85 Å) environments.

I. Introduction

The local environment of iron in amorphous ionocovalent compounds like oxide glasses has been studied by several techniques such as Mössbauer spectroscopy, optical absorption, and X-ray absorption spectroscopy (*1–4*). Very conclusive studies on this subject were made by Mössbauer spectroscopy on phosphate glasses in which iron has been generally reported in octahedral coordination whatever the valence state. In a recent study of iron-rich phosphate glasses by XAS, the presence of large amounts of Fe^{3+} in tetrahedral coordination has been observed by measurement of the prepeak intensity (*5*).

Thus the amorphization of ferrimagnetic oxides could be an interesting way of producing new local environments without any formatter. Although some garnets and spinels already have been amorphized by the splat cooling method (*6*), another way to amorphize ferrimagnetic oxides is to irradiate the compounds by high energy heavy ions in proper conditions (*7–10*). For instance, garnet $Y_3Fe_5O_{12}$, irradiated at room temperature by xenon ions of 3 GeV total energy, is completely amorphized when the fluence becomes large enough ($\Phi t \simeq 5 \times 10^{12}$ Xe · cm^{-2}). This result has been observed on Mössbauer spectra which show only a central paramagnetic doublet (*7, 8*) at room temperature and by high resolution electron microscopy (HREM) (*9, 10*). Heavy ion irradiation appears to be the

0022-4596/91 $3.00

only technique available, known up to now, to amorphize in bulk conditions compounds like the barium hexaferrite $BaFe_{12}O_{19}$.

In order to get some information about the local bonding around iron in this very disordered matter and to correlate with the frustrate magnetic properties recorded by magnetization measurements, Mössbauer and X-ray absorption spectroscopies were performed on xenon-irradiated amorphized garnet $Y_3Fe_5O_{12}$ and barium hexaferrite $BaFe_{12}O_{19}$.

II. Experimental

Sintered disks of both materials, $Y_3Fe_5O_{12}$ and $BaFe_{12}O_{19}$ (4 mm in diameter and 70–80 mm thick), were held against a thin aluminum foil perpendicular to the ion beam. A fluence of 5×10^{12} Xe · cm^{-2}, delivered by GANIL at 27 MeV/n, was necessary to completely amorphize the disks, especially in the case of $BaFe_{12}O_{19}$. The amorphousness of the irradiated samples was checked first by Mössbauer spectroscopy using a conventional apparatus equipped with a ^{57}Co in rhodium source: only a pure paramagnetic doublet was still observed at room temperature. An He flux cryostat was used to record the spectra at 5 K. The computer simulation was realized using a program written by J. Teillet and F. Varret from the University of Maine (France). Also on the same disks, X-ray diffraction patterns showed no lines and HREM the absence of any lattice plane resolution. The reproducibility of the amorphization of $BaFe_{12}O_{19}$ and $Y_3Fe_5O_{12}$ disks in the same irradiation conditions was checked several times so that, for the large surfaces needed by X-ray absorption spectroscopy (5×25 mm^2), a thin and regular layer of crystalline powder was spread on aluminum-coated adhesive ribbon and then directly irradiated at the same fluence.

XAS measurements have been performed at the EXAFS III beam line at LURE (Orsay). The Si (311) double-crystal monochromator was used over an energy range of 800 eV above the edge, with a 2-eV step. The edges were scanned using a 0.5-eV step. In order to minimize a Debye–Waller damping of the spectra, the samples were maintained at 30 K during the experiment. The energy calibration was obtained by setting the inflection point of the metallic iron K edge at 7112 eV. The samples studied were powders of $Y_3Fe_5O_{12}$ (YIG) and $BaFe_{12}O_{19}$ (BAF) irradiated and unirradiated (taken as reference), and of Fe_2O_3, $FePO_4$, Fe_3PO_7 (*11*), $YBaCuFeO_{5+\delta}$ (*12*), and $SrMn_{1-x}Fe_xO_{2.5}$ ($x = 0.15$) (*13*) taken as standards of iron in various oxygen environments.

III. Results and Discussion

A. Mössbauer Spectroscopy

Mössbauer spectra, realized at 5 K, are presented Figs. 1 and 2 for references with xenon-irradiated garnet and barium hexaferrite, respectively. Simulated spectra are plotted on the corresponding experimental curves and the parameters of the contribution are given in Table I.

The reference spectrum of the polycrystalline garnet (Fig. 1a), recorded at 5 K, has been simulated using two octahedral and one tetrahedral contribution as it is usually done (Table I). The theoretical abundances of octahedral (40%) and tetrahedral sites (60%) in the structure are reproduced by the fitting within 2%.

The reference spectrum of the polycrystalline barium hexaferrite (Fig. 2a), also recorded at 5 K, looks quite different from the crystallized garnet: it has been simulated using two octahedral sites (12*k* and $4f_2$), one tetrahedral site ($4f_1$), and one iron site with a particular environment (2*b*, triangular based bipyramids). From the structure determination, another octahedral site (2*a*) should be taken into account, but it is

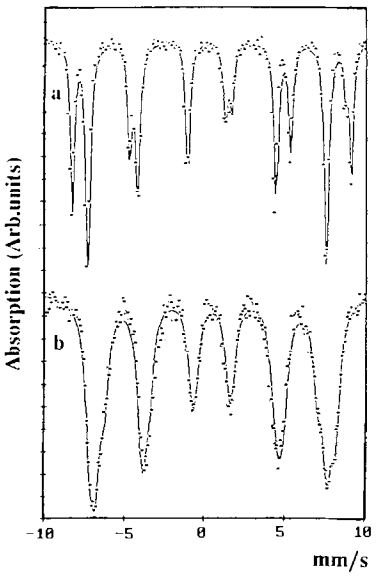

FIG. 1. (a) Mössbauer spectra of polycrystalline garnet $Y_3Fe_5O_{12}$ used as a reference at 5 K. (b) Amorphous xenon-irradiated garnet recorded at 5 K ($\Phi_t = 5 \times 10^{12}$ Xe · cm^{-2}, $E = 27$ MeV/n, $\langle (dE/dx)_e \rangle = 36$ MeV/μm).

TABLE I

MÖSSBAUER PARAMETERS[a] AND SITE CONCENTRATIONS RESULTING FROM THE FITTING OF EXPERIMENTAL SPECTRA FOR UNIRRADIATED AND XENON-IRRADIATED ($\Phi t = 5 \times 10^{12}$) Xe · cm^{-2}) FERRITES

Sample	Site	I.S.	Γ	2ε	H.F.	%
Crystalline	12*a*	0.49	0.15	0.11	542	31
$Y_3Fe_5O_{12}$,	4*a*	0.42	0.11	−0.04	527	7
sintered	24*d*	0.25	0.18	0.03	463	62
$Y_3Fe_5O_{12}$,	1	0.46	0.33	0.02	475	33
amorphous	2	0.40	0.36	−0.01	447	47
	3	0.38	0.30	−0.03	412	20
Crystalline	$4f_2$	0.50	0.18	0.18	551	27
$BaFe_{12}O_{19}$,	$4f_1$	0.38	0.22	0.12	527	24
sintered	12*k*	0.49	0.13	0.46	520	44
	2*b*	0.47	0.08	2.36	426	5
$BaFe_{12}O_{19}$,	1	0.50	0.23	0.18	516	10
amorphous	2	0.43	0.31	0.03	491	34
	3	0.42	0.31	0.01	466	38
	4	0.40	0.28	−0.02	437	18

[a] I.S., isomer shifts; Γ, linewidths; 2ε, quadrupolar effects (in mm/sec); H.F., hyperfine field (in kG). Isomer shifts are corrected for the iron shift (0.115 mm/sec) taken as a reference.

often mixed with the $12k + 4f_2$ contributions. The fitting of the parameters leads to 24% tetrahedral sites instead of the 17% theoretical abundance, probably because of a mixture of 2*a* and 2*b* with $4f_1$ and $4f_2$ sites. Thus one can find by Mössbauer spectroscopy the theoretical and relative amounts of tetrahedral and octahedral sites inside both structures within 8% precision.

The spectra of the irradiated compounds recorded at room temperature show only a paramagnetic doublet with large quadrupolar splitting and line width: electron diffraction and microscopy have shown that these irradiated compounds are completely amorphous (*9, 10*) and present very weak magnetization with magnetic properties characteristic of frustrated magnetic interactions which have been described elsewhere (*14*).

The Mössbauer spectrum of the amorphous garnet, recorded at 5 K (Fig. 1b), appears quite similar to the one obtained by

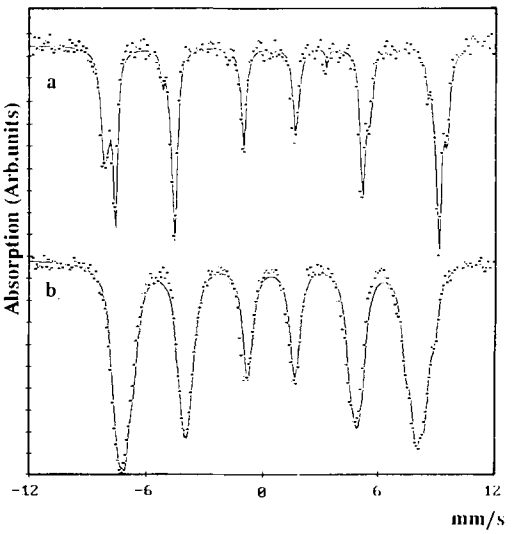

FIG. 2. (a) Mössbauer spectra of polycrystalline $BaFe_{12}O_{19}$ used as a reference at 5 K. (b) Amorphous xenon-irradiated $BaFe_{12}O_{19}$ recorded at 5K: same conditions as described in legend to Fig. 1a.

Eibschütz *et al.* (*6*) by a fast cooling method with large asymmetric lines which has been fitted by means of one mean isomer shift (0.446 mm/sec) and hyperfine field (450 kG). These authors concluded that the 4- and 6-coordinated Fe^{3+} ions disappeared with the predominance of a fivefold coordination of iron inside the amorphous garnet. Our simulations have shown that three contributions are necessary to fit the spectrum properly rather than a mean and broad one. These three contributions could correspond to octahedral, pyramidal, and tetragonal environments of iron but can also be interpreted as the main terms of a large distribution of iron and yttrium second neighbors centered on a mean fivefold coordination. As a matter of fact, the isomer shifts of these three contributions appear to stand between those of the octahedral and the tetrahedral sites in the reference compound. As is discussed in the next paragraph, iron has been observed by XAS in some crystallized oxides presenting a fivefold coordination, square pyramid, or trigonal bipyramid.

The Mössbauer spectrum of the amorphous barium hexaferrite (Fig. 2b) looks quite similar to the irradiated garnet spectrum: as in the latter case, attempts to simulate the spectrum of $BaFe_{12}O_{19}$ by a distribution of hyperfine fields and isomer shifts were not successful and a correct fit was obtained using four contributions, each of them being greater than 10% in relative intensity. The values of the isomer shifts are again intermediate between those of the octahedral and the tetrahedral sites, except for the first one, which may be considered as the remainder of the initial predominant octahedral sites in this structure. One can again interpret the simulation by means of the octahedral sites, which groups the first sites with the highest hyperfine field parameters, pyramidal and tetrahedral sites, or by using a large distribution of magnetic interactions based on a fivefold coordination with various numbers of iron ions as second neighbors and with large line widths due to the spreading of Fe–O bond lengths and angles.

Tentative analyses of the Mössbauer spectra of $Sr_2LaFe_3O_{8+y}$ and $Sr_2Fe_{2-x}Cr_xO_{5+y}$ oxygen-deficient perovskites in terms of local iron environment have been undertaken by T. C. Gibb and co-workers (*22, 23*). These authors tried to correlate the variations of isomer shifts, quadrupolar splittings, and magnetic hyperfine intensities with oxygen stoichiometries to the number of close neighbors. For that purpose, they found that isomer shift was the most relevant parameter: at 290 K, isomer shifts for Fe^{3+} in an octahedral environment stand around 0.38 mm/sec, 0.17 mm/sec in tetrahedra, and intermediate values around 0.28 mm/sec for fivefold coordination. Taking into account the observed 30% increase of isomer shifts between 290 and 5 K, the latter value leads to 0.4 mm/sec for fivefold-coordinated Fe^{3+} at 5 K, in good agreement with the present analysis of the spectra of the irradiated ferrites (see Table I).

Working on oxygen-deficient perovskites, the authors concluded that there is a square pyramidal environment around Fe^{3+} cations. Moreover, the existence of oxides such as $Ca_2Mn_2O_5$ (*24*) presenting layers of Mn^{3+} in square pyramid coordination allowed the assumption that Fe^{3+} and Fe^{4+} (same electronic configuration $3d^4$ as Mn^{3+}) occurred in the same type of environment. Nevertheless, the comparison of Mössbauer data is relevant only in isostructural compounds and did not give a definite answer about iron coordination in variable anion environments and structural types especially in highly disordered materials.

To further examine the problem of the local environment of iron, we performed X-ray absorption spectroscopy analysis of some crystallized reference compounds, chosen for their well-known structures, and the amorphous irradiated ferrites.

B. XAS

(1) *XANES at the Fe–K Edge*

The spectra were normalized when the step of the edge was fixed at 1; the step was evaluated as equal to the difference in absorption of the preedge and the high energy part of the spectra where there is no more EXAFS oscillation. The zero of energy was taken at the metallic Fe–K edge. The energy position of the edge of each sample was fixed at the inflection point of the main absorption jump. It was found to be nearly the same for all the samples and located at 13 ± 2 eV. It has been shown that the exact position of the inflection point for Fe compounds does not reflect only the valence state of the ion: M. Verdaguer *et al.* (*15*) have reported in iron porphyrins the same value for Fe(II) in square planar configuration and Fe(III) in square pyramidal configuration of iron porphyrins.

Fe_2O_3 and $FePO_4$ spectra were recorded as standards of Fe in octahedral and tetrahedral coordination, respectively (Fig. 3). $YBaCuFeO_{5+\delta}$ is an oxygen-deficient perovskite where Fe atoms are substituted to Cu and are in a square-based pyramidal configuration (*11*), with a fivefold coordination (symmetry group C_{4v}). The Fe_3PO_7 sample is also a compound where the Fe atoms are 5-coordinated but inside a trigonal bipyramid (group D_{3h}: Fig. 3). Another pyramidal compound was also studied: $Sr_2(Fe_{0.85}Mn_{0.15})_2O_5$. In this compound, the Mössbauer measurements (*13*) indicate that the Fe atoms which are substituted to Mn are 5-coordinated. However, no structural determination exists on this last sample.

(*a*) *Standard samples.* Figure 4a shows the spectra of the four former standards. All of these spectra have a preedge structure located at 2 eV (peak A in the figure). This preedge peak is commonly attributed to electronic transition from the $1s$ core level to orbitals with mainly $3d$ character (*16–18*) and has been used as a fingerprint to identify a noncentrosymmetric environment including tetrahedral coordination of Fe in oxide glasses (*5*). The interpretation for such a $1s$–$3d$ transition is generally an electric dipole transition to hybridized p–d states. This hybridization may be the result of the absence of an inversion center in the molecular cluster. A quadrupolar contribution to this preedge structure is also possible and has been evidenced in some cases by G. Dräger *et al.* (*19*). The XANES of several Fe compounds in 4-, 5-, and 6-coordination have also been studied by Berthet *et al.* (*18*). They have identified the different structures which appear on the edges of these compounds. In particular the compound $FePO_4$ has also been studied by these authors.

The most intense prepeak is observed for $FePO_4$ and in that case it is due to the lack of a center of symmetry in the FeO_4 tetrahedra. On the contrary, Fe_2O_3 has a small prepeak which has been shown by Dräger *et al.* to comprise quadrupole and dipole transitions, with a predominance of the dipole transition. In this compound Fe is in a slightly distorted octahedral coordination. This prepeak is split into two components, A_1 and A_2, which can be correlated to the splitting of the $3d(t_{2g}, e_g)$ orbitals in the octahedral crystal field.

The $YBaCuFeO_5$ and Fe_3PO_7 compounds are in an intermediate situation. Table II gives the intensity of the prepeak of the normalized spectra. The increasing order for the intensity of this prepeak is as follows: Fe_2O_3, $YCuFeO_5$, Fe_3PO_7, $FePO_4$ (Fig. 4a). This is consistent with the fact that the p–d hybridization must increase from the first to the last compound. In Fe_2O_3 the symmetry for the FeO_6 cluster is close to O_h, which implies no p–d hybridization. The small signal observed is due to the distortion of the octahedra plus the quadrupolar contribution as was said before.

In contrast, in $FePO_4$ the FeO_4 cluster is in T_d symmetry and the three p_x, p_y, p_z or-

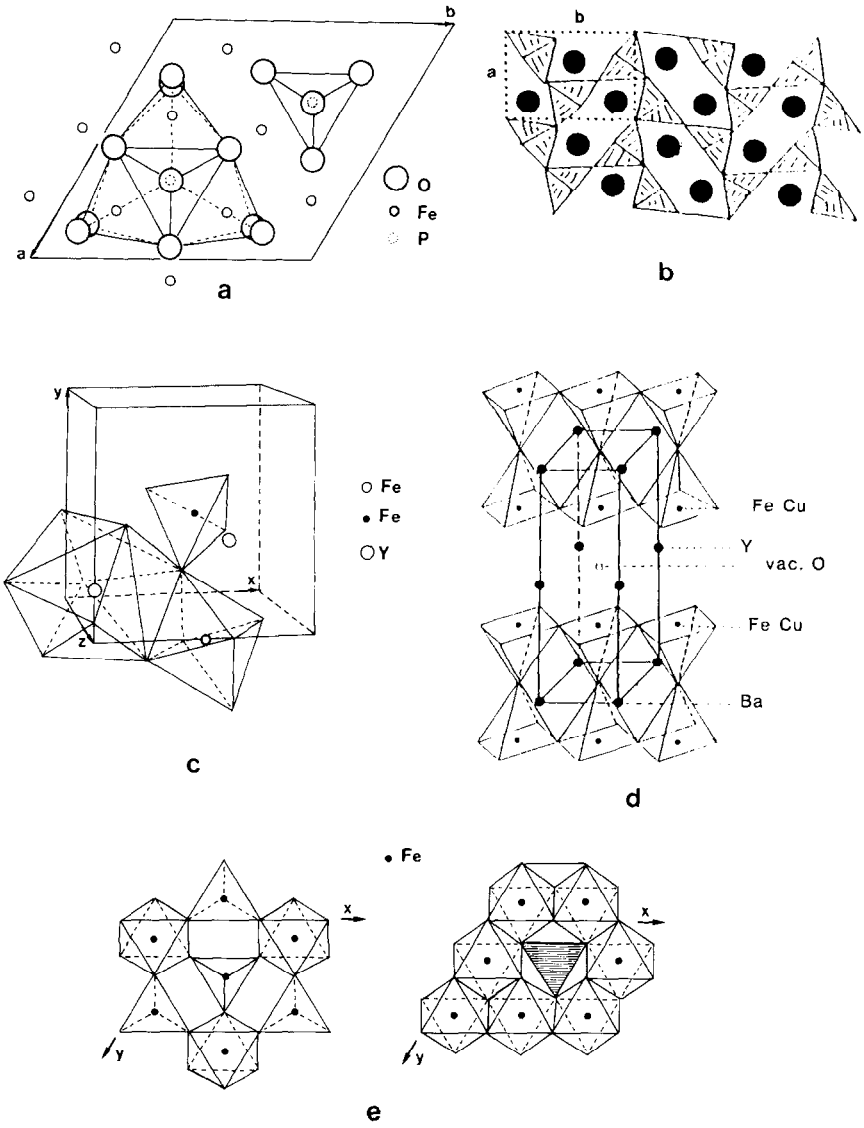

FIG. 3. Structural models showing the local order around iron for (a) Fe_3PO_7, projection down the c-axis showing the trigonal bipyramids around iron (11); (b) $Sr_2Mn_2O_5$, projection down the c-axis showing the square pyramids around iron (13); (c) $Y_3Fe_5O_{12}$, perspective view showing the 6 and 4 coordination around iron (14); (d) $YBaCuFeO_5$, perspective view showing the square pyramids around iron (13); (e) $BaFe_{12}O_{19}$, projection down the c-axis showing, left: mixed layer with 4 ($4f_1$)- and 6 ($2a$)-coordinated iron, right: Kagome layer with 6 ($12k$) coordinated iron and Kagome window K.

bitals are mixed with the three d_{xy}, d_{xz}, d_{yz} orbitals. In the case of $YBaCuFeO_5$ and Fe_3PO_7, the FeO_5 clusters are in C_{4v} and D_{3h} symmetry, respectively, and only the p_x and p_y are hybridized with the d orbitals. But for C_{4v}, p_x and p_y are hybridized with the d_{xz}, d_{yz} orbitals, whereas for D_{3h} the p_x and p_y are hybridized with $d_{x^2-y^2}$ and d_{xy}, and there exists a better overlapping of the d and p orbitals in this latter case since they

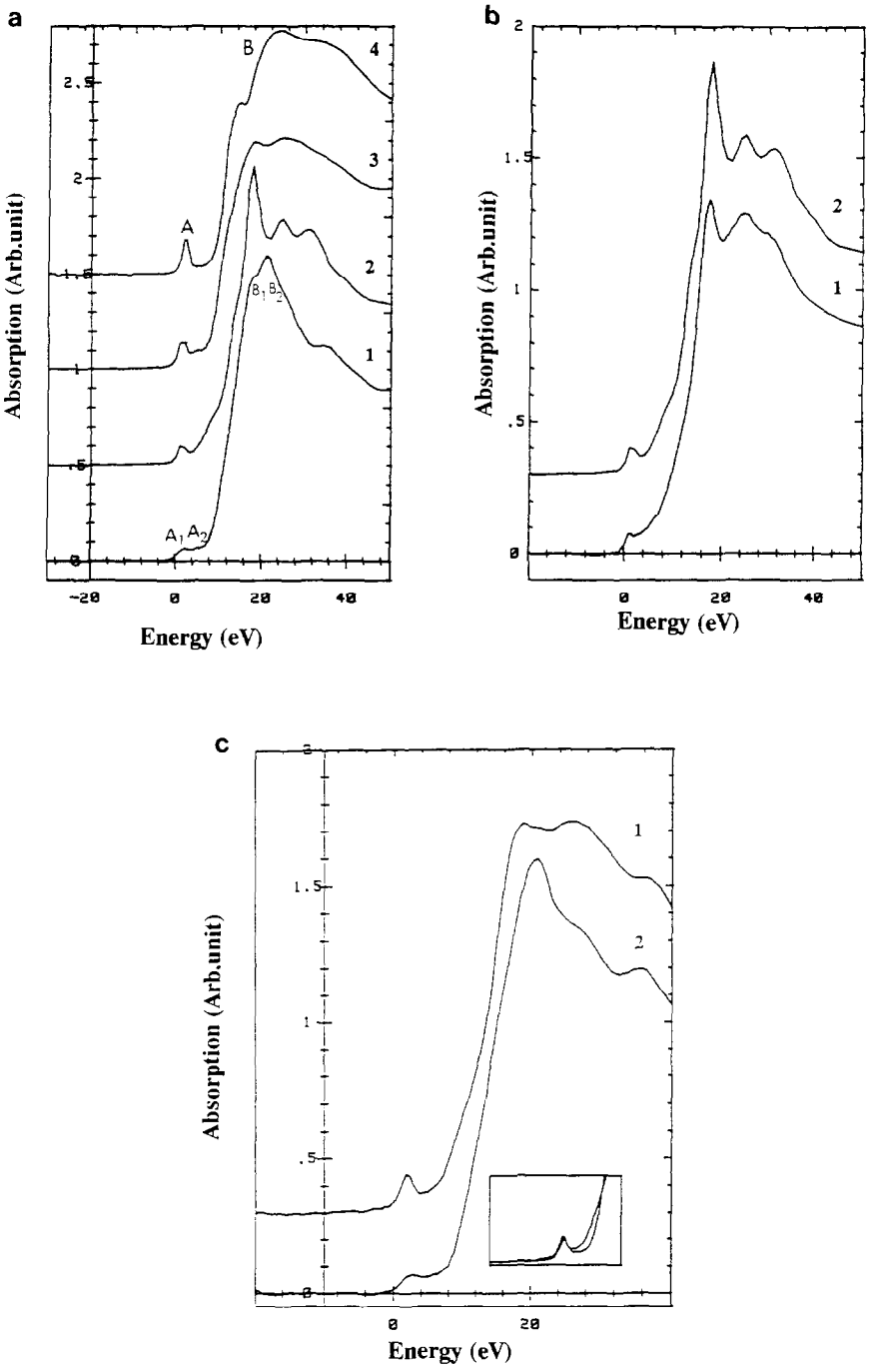

FIG. 4. (a) Absorption at Fe–K edge of Fe_2O_3, 1; $YBaFeCuO_5$, 2; Fe_3PO_7, 3; and $FePO_4$, 4. (b) Comparison of $YBaFeCuO_5$, 2; and $Sr_2(Mn_{0.15}Fe_{0.85})_2O_5$, 1. (c) Absorption spectra of the garnet $Y_3Fe_5O_{12}$, 1; and the barium hexaferrite $BaFe_{12}O_{19}$, 2. Inset, prepeak of YIG and of a combination of 60% $FePO_4$ and 40% Fe_2O_3.

TABLE II

COMPOSITIONS AND STRUCTURAL PARAMETERS OF SOME OXIDES WITH VARIOUS OXYGEN ENVIRONMENTS AND OF XENON-IRRADIATED FERRITES

Sample	Prepeak height	First neighbor N	EXAFS R(Å)	σ(Å^2)	X-ray R(Å)
Fe_2O_3	0.03	6	1.95	0.014	3 × 1.91 3 × 2.06
$FePO_4$	0.5	4	1.88	0	4 × 1.88 1 × 1.892
Fe_3PO_7	0.14	5	1.95	0.004	1 × 1.917 2 × 1.920 1 × 2.190 1 × 1.998
$YBaFeCuO_5$	0.06	5	1.98	−0.004	4 × 1.999 1 × 2.13 4 × 1.966
$SrMn_{0.85}Fe_{0.15}O_{2.5}$	0.05	5	1.91	−0.004	— 4 × 1.872
YIG, sintered	0.2	4	1.87	0.003	6 × 2.000
YIG, amorphous	0.12	5.	1.95	−0.001	—
BaF, sintered	0.03	6.0	1.93	0.014	—
BaF, amorphous	0.12	5.	1.96	0.002	—

lie in the same plane. This explains why the prepeak is more intense for Fe_3PO_7 than for $YBaCuFeO_5$.

The main absorption peak (B; Fig. 4a) is due to an s–p transition. The shape of the edge of $FePO_4$ is similar to that of the $[MnO_4]$ tetrahedra studied by Benfatto *et al.* (*22*). They show that multiple scattering with contributions of order higher than 3 is essential to reconstruct the B_1 and B_2 features. In the case of Fe_2O_3, the comparison with the $[MnO_6]$ octahedra studied by the same authors is not valid since the octahedra of Fe_2O_3 are slightly distorted. However, the main absorption peak B is very intense as is expected in octahedral symmetry. It is split into two components (B_1 and B_2: letters referring to Fig. 4a), which have been shown by Dräger *et al.* (*19*) to have z (B_1) and x, y (B_2) polarization. Thus the transitions can be attributed to p_z (B_1) at lower energy and p_x, p_y (B_2) at higher energy. In the case of the MnO_4 tetrahedra, Benfatto *et al.* have shown that the range of energy where the multiple scattering must be considered is about 120 eV, and only 60 eV for octahedra because of the cancellation of the third and fourth order contribution to multiple scattering in octahedra This corresponds to an energy of 120 $(d_{MnO}/d_{FeO})^2 = 80$ eV for the $[FeO_4]$ tetrahedra. $YBaCuFeO_5$ presents a very sharp B peak, which is also a $1s$–$4p$ transition. The $Sr_2(FeMn)_2O_5$ compound presents the same XANES spectrum as $YBaCuFeO_5$ and it can be concluded that for this sample the local symmetry around the Fe ions is the same (Fig. 4b).

(*b*) *Irradiated samples.* In Fig. 4c are presented the absorption spectra of the unirradiated ferrites. The $BaFe_{12}O_{19}$ unirradiated sample has a preedge similar to that of Fe_2O_3, which is consistent with the fact that in this compound the majority of Fe atoms are in octahedral configuration (*20*). The garnet $Y_3Fe_5O_{12}$ is an intermediate between $FePO_4$ and Fe_2O_3 and this is due to both tetrahedral and octahedral coordination of Fe atoms in the compound. It is possible to reconstitute the $Y_3Fe_5O_{12}$ prepeak with a linear combination of the two standards Fe_2O_3 and $FePO_4$ (Fig. 4c, inset). One finds 60% tetrahedra and 40% octahedra, in agreement with the crytallographic structure.

$BaFe_{12}O_{19}$ has the same sharp B peak as Fe_2O_3 corresponding to the octahedra with Fe–O distances varying from 1.93 to 2.06 Å. In contrast, $Y_3Fe_5O_{12}$ and $FePO_4$ present a round-shaped edge characteristic of a pure tetrahedral environment (*18*).

A comparison of irradiated and nonirradiated samples is shown in Figs. 5a ($Y_3Fe_5O_{12}$) and 5b ($BaFe_{12}O_{19}$). Both irradiated samples which had different preedge and XANES structures tend toward analogous spectra. The prepeak A decreases in intensity for the YIG compound and increases for the BAF compound, becoming intermediate between those of unirradiated BAF and YIG. If one assumes that in these amorphous compounds there is still a mix-

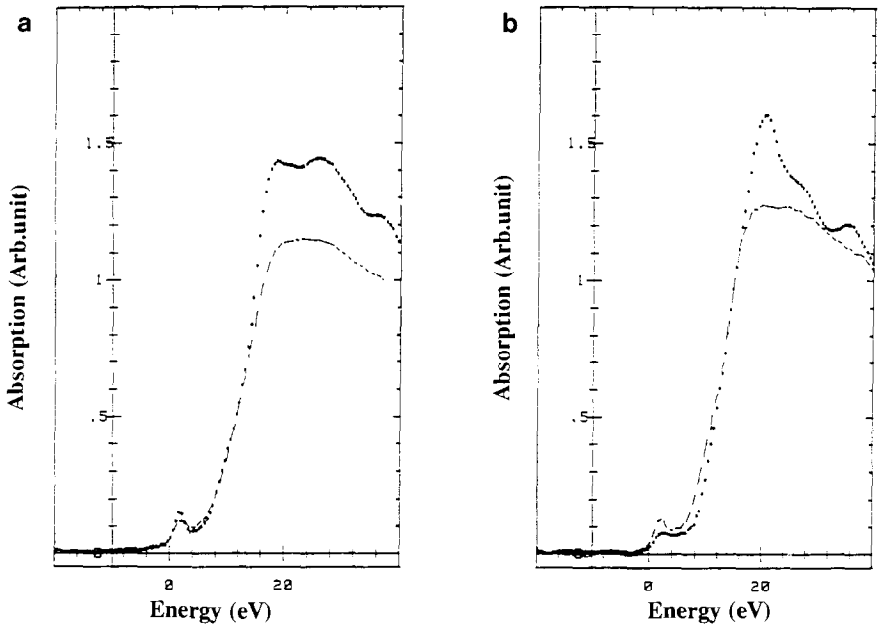

FIG. 5. (a) Absorption edges of irradiated (---) and unirradiated garnet (· · ·). (b) Same as (a) for BaF.

ture of tetrahedral and octahedral sites around Fe^{3+} cations, one finds that the irradiated samples have between 70 and 80% of octahedral sites by linear combinations of the prepeaks of Fe_2O_3 and $FePO_4$. However, it is not possible by this simulation to reconstruct the shoulder B observed in the irradiated samples. This shoulder appears only in the edge of the reference compound Fe_3PO_7 and the prepeak A intensity is in good agreement with those of the irradiated compounds (Fig. 6).

The XANES structures are completely washed out, as expected for an amorphous sample, and the intensity of the main transition peak is considerably lowered in the case of $BaFe_{12}O_{19}$.

(2) EXAFS Spectra

The EXAFS modulations were extracted using a standard method (*21*). The phase and amplitude of Fe–O were calculated

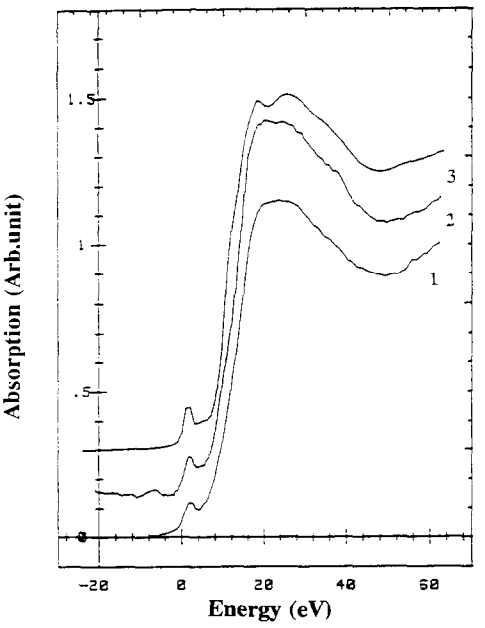

FIG. 6. Absorption at Fe–K edge of irradiated YIG, 1; BaF, 2; and of Fe_3PO_7, 3.

from $FePO_4$ taking four oxygen atoms surrounding the Fe atom at a distance of 1.85 Å.

The Fourier transforms of $k\chi(k)$ are presented in Fig. 7 for the irradiated and unirradiated samples. The first peak of the modulus of the Fourier transform corresponds to Fe–O distances. At a first examination, one can see that this peak decreases notably when $BaFe_{12}O_{19}$ becomes amorphous, but shows a small increase for $Y_3Fe_5O_{12}$. In addition, there is a small shift of the Fe–O peak in amorphous $Y_3Fe_5O_{12}$ toward longer distances, whereas there is no noticeable shift for $BaFe_{12}O_{19}$. This indicates that there is a change in the mean coordination number of Fe in both amorphous compounds but these changes are of opposite sign. One can observe also a quasicancellation of the second peak of distances, which is expected from an amorphous sample.

Since the Fourier transform was taken at 80–450 eV because of the limitations at low energy due to multiple scattering, only single shell-fittings of the Fourier transforms of the first peak were tested. The significant results are the distances in the shell, the coordination number being correlated with the Debye–Waller factor. The number of oxygen neighbors around iron was arbitrarily fixed at five atoms in the irradiated samples, four in the unirradiated garnet, and six in the unirradiated $BaFe_{12}O_{19}$. One observes in the garnet that the Fe–O distances change from 1.87 Å, characteristic of tetrahedra, to 1.95 Å, more characteristic of octahedral or fivefold coordination after amorphization. In the case of the barium hexaferrite, the distances change from 1.93 Å, which corresponds to the shortest Fe–O distances in the octahedra (*20*), to 1.96 Å. This variation is the limit of sensitivity of the experiment. Nevertheless, one can say that there is no detectable emergence of short distances as in tetrahedra despite the fact that the prepeak is enhanced and the

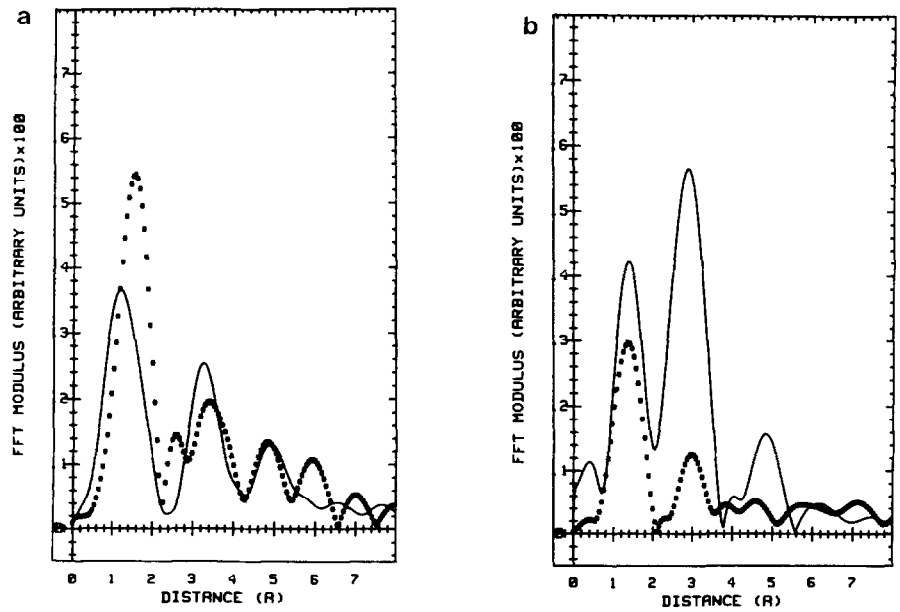

FIG. 7. (a) Fourier transform of EXAFS $k\chi(k)$ spectra of unirradiated (continuous line) and irradiated (dotted line) YIG. (b) Same as (a) for BaF.

modulus of the Fourier transform is noticeably decreased in this last compound. These results lead us to the conclusion that iron atoms are fivefold coordinated in the amorphous samples. The same type of fitting realized on Fe_3PO_7 yields a mean Fe–O distance of 1.95 Å and on $YBaCuFeO_5$ and $Sr_2(Fe_{0.85}Mn_{0.15})_2O_5$ compounds of 1.98 Å. These distances are close to the ones observed in the amorphous samples.

C. Discussion

Both the edge and the EXAFS comparisons of irradiated and unirradiated ferrites indicate that the amorphization induced by high energy heavy ions leads to a fivefold coordination of iron close to a trigonal bipyramid configuration as in Fe_3PO_7. Moreover, the X-ray absorption spectra of both xenon-irradiated amorphized compounds look very close to one another, yielding the same amorphous phase for the two kinds of ferrites although their initial structures are different. Taking into account such a result, the strong decrease of the hyperfine field in the main contributions to the Mössbauer spectra can be interpreted on the basis of a variable number of iron second neighbors since magnetic coupling arises from superexchange interactions via the oxygen ligands. For instance, in the irradiated garnet, the three contributions could correspond respectively to 5, 4, and 3 iron second neighbors with the corresponding decrease of the hyperfine field (Table I). The same result can be proposed for the irradiated barium hexaferrite, except for the first contribution (Table I) which presents the weakest intensity and the strongest hyperfine field and is likely due to a remainder of iron in octahedral coordination. This last observation can be related to the smaller sensitivity to heavy ion irradiation of $BaFe_{12}O_{19}$ with respect to the garnet, which has been shown by Ch. Houpert *et al.* (*21*) in their Mössbauer study of irradiation damage in magneto-plumbite-type structures. These authors observed that $12k$ octahedral sites remained in the Mössbauer spectra of the irradiated samples until complete amorphization when $4f_1$, $4f_2$, and $2b$ sites vanished at lower fluences.

Thus it appears that, in the amorphous ferrites, iron atoms take a well-defined fivefold coordination with oxygen first neighbors forming a trigonal bipyramid but, as soon as second neighbors are considered, the order vanishes and a distribution of cations, bond lengths, and angles occurs. This type of local ordering will create multiple magnetic interactions which result in frustrated magnetic properties observed by magnetization and susceptibility measurements (*14*).

References

1. M. Darby Dyar, *Amer. Mineral.* **70,** 304 (1985).
2. A. M. Bishay and L. Makar, *J. Amer. Ceram. Soc.* **52,** 605 (1969).
3. R. S. Motran, A. M. Bishay, and D. P. Johnson, "Recent Advances in Science and Technology of Materials" (A. Bishay, Ed.), Vol. 1, p. 109, Plenum Press, New York (1973).
4. F. Mesnil, L. Fournes, J. M. Dance, and J. J. Videau, *J. Phys. Colloq. C1(1),* **41,** c1–271 (1980).
5. F. Studer and A. Le Bail, *J. Phys. Colloq. C8 Suppl 12* **47,** c8–781 (1986).
6. M. Eibschütz and M. E. Lines, *Phys. Rev. B* **26**(4), 1043 (1982).
7. M. Toulemonde, D. Groult, N. Nguyen, and F. Studer, *Phys. Rev. B* **35**(13), 6560 (1986).
8. F. Studer, D. Groult, N. Nguyen, and M. Toulemonde, *Nucl. Instrum. Methods Sect. B* **19/20,** 856 (1987).
9. G. Fuchs, F. Studer, E. Balanzat, D. Groult, M. Toulemonde, and J. C. Jousset, *Europhys. Lett.* **3,** 321 (1987).
10. Ch. Houpert, M. Hervieu, D. Groult, F. Studer, and M. Toulemonde, *Nucl. Instrum. Methods Sect. B* **32** 393 (1988).
11. A. Modaressi, A. Courtois, R. Gerardin, B. Malaman, and Ch. Gleitzer, *J. Solid State Chem.* **47,** 245 (1983).
12. L. Er-Rakho, C. Michel, Ph. Lacorre, and B. Raveau, *J. Solid State Chem.* **73,** 4056 (1988).
13. V. Caignaert, N. Nguyen, M. Hervieu, B. Raveau, *Mater. Res. Bull.* **20,** 479 (1985).

14. CH. HOUPERT, Thèse d'Université, CAEN (1989).
15. M. VERDAGUER, C. CARTIER, M. MOMENTEAU, E. DARTYGE, A. FONTAINE, G. TOURILLON, AND A. MICHALOWICZ, *J. Phys. C*8, **47,** 649 (1986).
16. J. PETIAU AND G. CALAS, *J. Phys. C*9 **43,** 47 (1982).
17. A. BIANCONI, E. FRITCH, G. CALAS, AND J. PETIAU, *Phys. Rev. B* **32,** 4292 (1985).
18. P. BERTHET, J. BERTHON, AND F. D'YVOIRE, *Mater. Res. Bull.* **33,** 1501 (1988).
19. G. DRÄGER, R. FRAHM, G. MATERLICK, AND O. BRÜMMER, *Phys. Status Solidi* **146,** 287 (1988).
20. W. TOWNES, J. FANG, AND A. PERROTA, *Z. Kristallogr.* **125,** 437 (1967).
21. CH. HOUPERT, N. NGUYEN, F. STUDER, D. GROULT, AND M. TOULEMONDE, *Nucl. Instrum. Methods Sect. B* **32** 393 (1988).
22. P. D. BATTLE, T. C. GIBB, AND S. NIXON, *J. Solid State Chem.* **79,** 75 (1989).
23. T. C. GIBB AND M. MATSUO, *J. Solid State Chem.* **86,** 164 (1990).
24. K. R. POEPPELMEIER, M. E. LEONOWICZ, AND J. M. LONGO, *J. Solid State Chem.* **44,** 89 (1982).